



The root-knot nematode effector MiEFF18 interacts with the plant core spliceosomal protein SmD1 required for giant cell formation

Joffrey Mejias, Jérémie Bazin, Nhat-my Truong, Yongpan Chen, Nathalie Marteu, Nathalie Bouteiller, Shinichiro Sawa, Martin Crespi, Hervé Vaucheret, Pierre Abad, et al.

► To cite this version:

Joffrey Mejias, Jérémie Bazin, Nhat-my Truong, Yongpan Chen, Nathalie Marteu, et al.. The root-knot nematode effector MiEFF18 interacts with the plant core spliceosomal protein SmD1 required for giant cell formation. *New Phytologist*, 2021, 229 (6), pp.3408-3423. 10.1111/nph.17089 . hal-03148749

HAL Id: hal-03148749

<https://hal.inrae.fr/hal-03148749>

Submitted on 8 Dec 2021

HAL is a multi-disciplinary open access archive for the deposit and dissemination of scientific research documents, whether they are published or not. The documents may come from teaching and research institutions in France or abroad, or from public or private research centers.

L'archive ouverte pluridisciplinaire **HAL**, est destinée au dépôt et à la diffusion de documents scientifiques de niveau recherche, publiés ou non, émanant des établissements d'enseignement et de recherche français ou étrangers, des laboratoires publics ou privés.

The Root-Knot Nematode Effector MiEFF18 interacts with the Plant Core Spliceosomal Protein Smd1 Required for Giant Cell Formation

Joffrey Mejias¹, Jérémie Bazin², Nhat-My Truong^{1,3}, Yongpan Chen^{1,4}, Nathalie Marteu¹, Nathalie Bouteiller⁵, Shinichiro Sawa³, Martin D. Crespi², Hervé Vaucheret⁵, Pierre Abad¹, Bruno Favery^{1,*} and Michaël Quentin^{1,*}

*** co-corresponding authors**

¹ INRAE, Université Côte d'Azur, CNRS, ISA, F-06903 Sophia Antipolis, France

² Institute of Plant Sciences Paris-Saclay (IPS2), CNRS, INRA, Universités Paris Saclay,-, Evry, Université de Paris, 91192 Gif sur Yvette, France

³ Graduate School of Science and Technology, Kumamoto University, Kumamoto 860-118555, Japan

⁴ Department of Plant Pathology and Key Laboratory of Pest Monitoring and Green Management of the Ministry of Agriculture, China Agricultural University, Beijing, China

⁵ Institut Jean-Pierre Bourgin, INRAE, AgroParisTech, Université Paris-Saclay, 78000 Versailles, France

*** Authors for correspondence**

Dr. Michaël Quentin

400 route des chappes, BP 167, 0690 Sophia Antipolis, France

Tel: +33 492386495

Email: michael.quentin@inrae.fr

Dr. Bruno Favery

400 route des chappes, BP 167, 0690 Sophia Antipolis, France

Tel: +33 492386464

Email: bruno.favery@inrae.fr

Joffrey Mejias, joffrey.mejias@etu.univ-cotedazur.fr, <https://orcid.org/0000-0001-7663-0314>

Jérémie Bazin, jeremie.bazin@universite-paris-saclay.fr

Nhat-My Truong, truongnhatmy@gmail.com, <https://orcid.org/0000-0003-2436-7897>

Yongpan Chen, chenyongpan1@163.com, <https://orcid.org/0000-0001-9074-7199>
Nathalie Marteu, nathalie.marteu@inrae.fr
Nathalie Bouteiller, nathalie.bouteiller@inrae.fr
Shinichiro Sawa, sawa@kumamoto-u.ac.jp, <https://orcid.org/0000-0002-9309-9104>
Martin D. Crespi, martin.crespi@universite-paris-saclay.fr, <https://orcid.org/0000-0002-5698-9482>
Hervé Vaucheret, herve.vaucheret@inrae.fr, <https://orcid.org/0000-0002-9986-0988>
Pierre Abad pierre.abad@inrae.fr, <https://orcid.org/0000-0003-0062-3876>
Bruno Favery bruno.favery@inrae.fr, <https://orcid.org/0000-0003-3323-1852>
Michael Quentin michael.quentin@inrae.fr, <https://orcid.org/0000-0002-8030-1203>

Total word count

6,853 words (Introduction, 897; Materials and Methods, 1823; Results, 2143; Discussion, 1775; Acknowledgements, 234).
Figures: 5 (All figures in colour).
Supporting information files: 23 (12 tables and 11 figures).

Summary

- The root-knot nematode *Meloidogyne incognita* secretes specific effectors (MiEFF) and induces the redifferentiation of plant root cells into enlarged multinucleate feeding "giant cells" essential for nematode development.
- Immunolocalisations revealed the presence of the MiEFF18 protein in the salivary glands of *M. incognita* juveniles. *In planta*, MiEFF18 localizes to the nuclei of giant cells demonstrating its secretion during plant-nematode interactions. A yeast two-hybrid approach identified the nuclear ribonucleoprotein SmD1 as a MiEFF18 partner in tomato and *Arabidopsis*. SmD1 is an essential component of the spliceosome, a complex involved in pre-mRNA splicing and alternative splicing.
- RNA-seq analyses of *Arabidopsis* roots ectopically expressing MiEFF18 or partially impaired in SmD1 function (*smd1b* mutant) revealed the contribution of the effector and its target to alternative splicing and proteome diversity. The comparison with *Arabidopsis* galls data showed that MiEFF18 modifies the expression of genes important for giant cells ontogenesis, indicating that MiEFF18 modulates SmD1 functions to facilitate giant cell formation.
- Finally, *Arabidopsis smd1b* mutants exhibited less susceptibility to *M. incognita* infection, and the giant cells formed on these mutants displayed developmental defects, suggesting that SmD1 plays an important role in the formation of giant cells and is required for successful nematode infection.

Key words: *Meloidogyne incognita*, Effector, Nucleus, Alternative Splicing, *Arabidopsis thaliana*, *Nicotiana benthamiana*

Introduction

Pathogens have evolved an arsenal of molecules known as effectors, which are secreted *in planta* to manipulate host functions and ensure successful infection. One striking example of plant cell manipulation is provided by the plant-parasitic root-knot nematodes (RKN) of the genus *Meloidogyne*. After penetrating the root and migrating to the vascular cylinder, the microscopic vermiform second-stage juveniles (J2s) induce the transformation of selected vascular root cells into specialised hypertrophied and multinucleate feeding cells. These ‘giant cells’ result from successive nuclear divisions without cell division, followed by isotropic cell growth (Favery *et al.*, 2016). They are several hundred times larger than normal root cells, contain about 50 to 100 endoreduplicated nuclei and have an expanded endoplasmic reticulum and numerous organelles (de Almeida Engler & Gheysen, 2013). Giant cells are surrounded by dividing cells, some of which differentiate into new xylem and phloem cells (Bartlem *et al.*, 2014), leading to the formation of a new organ, the gall. Giant cells act as a strong metabolic sink and are the sole source of nutrients for the nematode during the sedentary part of its life cycle in the plant. The pear-shaped RKN females eventually lay their eggs on the root surface. Interestingly, RKN can induce giant cells in more than 4,000 plant species, probably by manipulating conserved plant functions (Singh *et al.*, 2013).

The major modifications observed in giant cells require extensive transcriptional reprogramming in root cells. Giant cell formation has been explored at the transcriptomic level in several plant-RKN interactions, and thousands of differentially expressed genes (DEG) have been identified in plants (Cabrera *et al.*, 2014; Yamaguchi *et al.*, 2017; Shukla *et al.*, 2018; Postnikova *et al.*, 2015; Favery *et al.*, 2016). Functional analyses of these genes have highlighted the key roles of microtubule and actin cytoskeleton rearrangements and cell cycle control in the formation of these multinucleate feeding cells (de Almeida Engler & Favery, 2011; de Almeida Engler & Gheysen, 2013; Favery *et al.*, 2016; Cabral *et al.*, 2020). Recent studies have shown that small non-coding RNAs, such as microRNAs (miRNAs) and small interfering RNAs (siRNAs), play a role in gall development (Jaubert-Possamai *et al.*, 2019).

The molecular mechanisms underlying giant cell formation remain poorly understood. It is assumed that effectors, including, in particular, proteins secreted *in planta* from the three oesophageal gland cells through a hollow protrusive stylet, are responsible for giant cell ontogenesis (Mitchum *et al.*, 2013; Truong *et al.*, 2015; Mejias *et al.*, 2019). Various

approaches, based on proteomics, transcriptomics and genomics, have been used to characterise RKN effector repertoires. The sequencing of *M. incognita* mRNAs isolated from gland cells or from parasitic juveniles *in planta* led to the identification of genes encoding putative effector proteins expressed specifically in the oesophageal gland cells and more strongly *in planta*, such as the *Minc18636/Minc15401* genes (Rutter *et al.*, 2014; Nguyen *et al.*, 2018). The expression in the oesophageal glands of about a hundred RKN effectors has been validated by *in situ* hybridisation (ISH), but secretion *in planta* has been demonstrated for only a few candidate effectors, by immunolocalisation (Truong *et al.*, 2015). Three RKN effectors have been shown to accumulate in the nucleus of giant cells (Jaouannet *et al.*, 2012; Lin *et al.*, 2012; Chen *et al.*, 2017). This targeting event in the host nucleus reflects the need for various nuclear processes, including transcriptional regulation, to be manipulated, to divert plant cell fate and disrupt immunity, as reported for other plant pathogens (Deslandes & Rivas, 2011; Motion *et al.*, 2015). Most RKN candidate effectors are ‘pioneers’ displaying no significant sequence similarity to any protein in databases and with no known functional domains; as a result, the functions of only a few RKN effectors have been deciphered (Mejias *et al.*, 2019). The *M. incognita* 7H08 effector has been shown to have transcriptional activity *in planta*, but the target genes in the host have yet to be identified (Zhang *et al.*, 2014). The 16D10 effector from *M. incognita* targets Scarecrow-like transcription factors (Huang *et al.*, 2006). In sedentary endoparasitic cyst nematodes, the GLAND4 effector has been shown to have transcriptional repressor activity against the promoters of two lipid transfer genes involved in plant defence (Barnes *et al.*, 2018). The 32E03 effector has epigenetic activity, through the inhibition of *Arabidopsis thaliana* histone deacetylases, thereby modulating host rDNA gene expression and promoting infection (Vijayapalani *et al.*, 2018).

Alternative splicing (AS) is a mechanism by which different forms of mature messenger RNA (mRNA) are generated from the same gene, from specific transcripts or through the deletion or retention of an exon/intron sequence (Wilkinson & Charenton, 2020). This regulatory mechanism results in the production of several related proteins, or isoforms, thereby increasing proteomic diversity. Plant pathogens have been shown to modulate AS (Rigo *et al.*, 2019). We show here that the MiEFF18 effector from *M. incognita* accumulates in the plant cell nucleus and interacts with an essential component of the spliceosome machinery, the small ribonucleoprotein particle SmD1, in tomato and *Arabidopsis*. Using a genome-wide transcriptome analysis, we found that MiEFF18 modulated AS, and gene expression, through a partial impairment of SmD1 activity. We also found that related

alternative splicing events occur in *Arabidopsis* upon nematode parasitism. Our findings further demonstrate that SmD1 is required for RKN infection and giant cell formation. Thus, MiEFF18 may contribute to giant cell development by modulating the function of a key component of the spliceosome to promote nematode infection.

Materials and methods

Plant material and growth conditions

All the *A. thaliana* plants used here were of the Columbia 0 ecotype (Col-0). The *smd1a* and *smd1b* mutants have been described elsewhere (Elvira-Matelot *et al.*, 2016). Seeds of *A. thaliana* Col-0, mutant and transgenic lines were surface-sterilised and sown on Murashige and Skoog (Duchefa) agar plates (0.5 x MS salts, 1% sucrose, 0.8% agar, pH 6.4) or in a mixture of soil and sand. Sowings were incubated at 4°C for two days, and then transferred to a growth chamber with an 8 h photoperiod, at 21°C. For propagation and transformation, seedlings were transferred to a growth chamber with a 16 h photoperiod, at 21°C. *A. thaliana* were transformed by the floral dip method (Bent & Clough, 1998). Homozygous transformed T3 plants were used. *Nicotiana benthamiana* plants were grown on soil, under a 16 h photoperiod, at 24°C. For the production of plant material for RNA-seq experiments, seeds were surface-sterilized and sown in liquid MS medium (0.5 x MS salts, 1% sucrose, pH 6.4) with gentle shaking (70 rpm), under a 12 h photoperiod, at 25°C. Roots were collected after 11 days and immediately frozen in liquid nitrogen until RNA extraction.

RKN infection assay

M. incognita strain “Morelos” was multiplied on tomato (*Solanum lycopersicum* cv. “Saint Pierre”) growing in a growth chamber (25°C, 16 h photoperiod). Freshly hatched J2s were collected as previously described (Caillaud & Favery, 2016). Three-week-old *Arabidopsis* seedlings were inoculated with 200 *M. incognita* J2s per plant. Roots were collected six weeks after infection and stained with 0.5% eosin. The number of females forming egg masses and root weight were then determined (n=25 to 40 plants per replicates). Three independent biological replicates were established for each set of conditions. Statistical analyses were carried out with R software (R Development Core Team, version 3.1.3). The effect of plant genotype on the number of nematode egg masses was analyzed with generalised linear models (GLMs) based on a Poisson distribution, for each replicate. We

used the Tukey adjustment method ('multcomp' package) for multiple testing. For giant cell area measurements, galls were collected 14 days post-infection (dpi), cleared in benzyl alcohol/benzyl benzoate (BABB) as previously described (Cabrera *et al.*, 2018) and examined under an inverted confocal microscope (model LSM 880; Zeiss). The mean areas of giant cells in each gall, for each genotype, and for two biological replicates, were measured with Zeiss ZEN software ($n = 42$ and 25 galls for Col-0 and *smd1b*, respectively). The impact of the plant genotype on the giant cell surface was analyzed using student t test since the dependent variables followed a Normal distribution using a Shapiro-Wilk Test.

Plasmid constructs

The *M. incognita* *MiEFF18* and *MiEFF16* coding sequences (CDS) lacking the signal peptide, the *S. lycopersicum* *SmD1*, *A. thaliana* *SmD1a* and *SmD1b*, the SV40 Antigen T, and the human P53 sequence were amplified by PCR with specific primers (Table S1) and inserted into the pDON207 donor vector. They were recombined in pK2GW7 (P35S:MiEFF18), pK7WGR2 (P35S:mRFP-MiEFF18), pK7FGW2 (P35S:eGFP-SlSmD1, P35S:eGFP-MiEFF16) or BiFC (pAM-35SS:GWY-YFPc, pAM-35SS:GWY-YFPn, pAM-35SS:YFPc-GWY, pAM-35SS:YFPn-GWY) or, for Y2H, the pB27-GW and pP6-GW (Karimi *et al.*, 2007; Caillaud *et al.*, 2009), with Gateway technology (Invitrogen). All the constructs were sequenced (GATC Biotech) and transferred into either *Agrobacterium tumefaciens* strain GV3101 or *Saccharomyces cerevisiae* strain L40ΔGal4 or Y187.

N. benthamiana agroinfiltration

Transient expression was achieved by infiltrating *N. benthamiana* leaves with *A. tumefaciens* GV3101 strains harbouring GFP- or mRFP-fusion or BiFC constructs, as previously described (Caillaud *et al.*, 2009). Leaves were imaged 48 hours after agroinfiltration, with an inverted confocal microscope equipped with an Argon ion and HeNe laser as the excitation source. For simultaneous GFP/mRFP imaging, samples were excited at 488 nm for GFP and 543 nm for mRFP, in the multi-track scanning mode. GFP or YFP emission was detected selectively with a 505-530 nm band-pass emission filter. We detected mRFP fluorescence in a separate detection channel, with a 560-615 nm band-pass emission filter.

Sequence analysis and alignment

M. incognita sequences were obtained from *Meloidogyne* genomic resources (http://www6.inra.fr/meloidogyne_incognita/). We used the MAFFT on the EBI server (<https://www.ebi.ac.uk/Tools/msa/mafft/>) for sequence alignment. The protein sequences encoded by the genes were analysed with PHOBIUS (<http://phobius.sbc.su.se/>), PSORT II (<http://psort.hgc.jp/form2.html>) and NoD (<http://www.compbio.dundee.ac.uk/www-nod/>) software, for the prediction of signal peptides, non-transmembrane domains, DNA-binding domains, NLS and NoLS, respectively. BLASTp analyses were carried out with an e-value threshold of 0.01 and without low complexity against the NCBI non-redundant protein database, for homologue identification. Interproscan was performed on the proteins to identify protein signatures referenced in the InterPro database (Mitchell *et al.*, 2015).

Yeast two hybrid

For the yeast two-hybrid (Y2H) screens, the coding sequences of the MiEFF18 and MiEFF16 effectors without their secretion signals and the *SlSmD1* CDS were inserted into pB27 as C-terminal fusions with LexA. The constructs were verified by sequencing and used to transform the L40ΔGal4 (MAT α) yeast strain. MiEFF18 was used as a bait in a mating approach, to screen a random-primed cDNA library from tomato roots infected with *M. incognita* and *Ralstonia solanacearum* carried by the Y187 (MAT α) yeast strain (Hybrigenics Services, Paris, France). Diploids carrying interactions were selected on a minimal synthetic defined SD medium lacking tryptophan (W), leucine (L) and histidine (H). The prey fragments of the positive clones were amplified by PCR and their 5' junctions were sequenced. The resulting sequences were used to identify the tomato interacting proteins with the Sol Genomics Network (<https://solgenomics.net/>) blast analysis tools. For pairwise Y2H assays, full-length controls, baits and candidate targets (MiEFF18 w/o SP, MiEFF16 w/o SP, *SlSmD1*, *AtSmD1a*, *AtSmD1b*, Antigen T and P53) were inserted into the pB27 or pP6 vector as C-terminal fusions with LexA or Gal4-AD, respectively, verified by sequencing and used to transform L40ΔGal4 (MAT α) or Y187 (MAT α) yeast strain. After mating between Y187 and L40ΔGal4, diploids were selected on medium lacking tryptophan and leucine, and interactions were tested on medium lacking tryptophan, leucine and histidine and supplemented with 0.5 mM 3-amino-1,2,4-triazole (3-AT).

Western blotting and immunolocalisation

MiEFF18 was inserted into the pET-24a (+) expression vector (Addgene), expressed in BL21star (DE3) cells, and purified on HisTrap FF columns (GE Healthcare Life Science). The purified protein was used to raise polyclonal antibodies in rabbits (Agro-Bio, La Ferté Saint Aubin, France). Western blotting was performed to check the specificity of the antibody as previously described (Zhao *et al.*, 2019b). Proteins were transferred onto a nitrocellulose membrane with the Trans-Blot Turbo Transfer system (Biorad). The membranes were blocked and incubated with α -MiEFF18 antibody (1:5,000 or 1/10,000) and then with goat anti-rabbit secondary antibodies coupled to horseradish peroxidase (HRP; 1:10,000).

Immunolocalisation was performed directly on *M. incognita* pre-parasitic J2s with the anti-MiEFF18 primary antibody (1:50) and a goat anti-rabbit Alexa Fluor 488-conjugated secondary antibody (1:200) (Molecular Probes) as previously described (Jaubert *et al.*, 2005). Pre-immune serum was used as a negative control. For *in planta* immunolocalisation, the antibodies were affinity-purified (Agro-Bio, La Ferté Saint Aubin, France) and used to performed immunolocalisation on Arabidopsis gall sections (14 dpi) with the anti-MiEFF18 purified antibody (1:500) and a goat anti-rabbit Alexa Fluor 488-conjugated secondary antibody (1:200) (Molecular Probes) as previously described (Zhao *et al.*, 2019). Images were collected with an inverted confocal microscope (model LSM 880; Zeiss).

Gene expression and alternative splicing analysis

Arabidopsis gall and non-infected control root RNA-seq data were generated and described in a previous study (Yamaguchi *et al.*, 2017). Total RNA was extracted from the roots of the three *Arabidopsis* lines (Col-0, P35S:MiEFF18 and *smd1b*) with TriZol (Invitrogen), according to the Invitrogen protocol. The RNA was treated with DNase treatment (Ambion), and its quality and integrity were assessed with a Bioanalyzer (Agilent). Libraries were constructed with the Tru-Seq Stranded mRNA Sample Prep kit (Illumina®). Paired-end sequencing with 75-bp reads was performed on a NextSeq500 perform. A minimum of 30 million paired-end reads per sample was generated. RNA-seq preprocessing included the trimming of library adapters and quality controls with Trimmomatic. Paired-end reads with a Phred Quality Score Qscore > 20 and a read length > 30 bases were retained, and ribosomal RNA sequences were removed with SortMeRNA. Processed reads were aligned using Tophat2 with the following arguments: --max-multihits 1 -i 20 --min-segment-intron 20 --min-coverage-intron 20 --library-type fr-firststrand --microexon-search -I 1000 --max-segment-intron 1000 --max-coverage-intron 1000 --b2-very-sensitive. Reads overlapping

exons were counted per gene with the FeatureCounts function of the Rsubreads package, using the GTF annotation files from the Araport11 repository (https://www.araport.org/downloads/Araport11_Release_201606/annotation/Araport11_GFF3_genes_transposons.201606.gff.gz). The significance of differential gene expression was estimated with DESeq2, with FDR correction of the p -value during pairwise comparisons between genotypes. A gene was considered to be differentially expressed if its adjusted p -value (FDR) was ≤ 0.01 . Transcripts were quantified on the basis of pseudo-alignment counts with kallisto on AtRTD2 transcript sequences (https://ics.hutton.ac.uk/atRTD/RTD2/AtRTDv2_QUASI_19April2016.fa) with a K -mer size of 31 nucleotides. Differential AS events in the AtRTD2 database were detected with SUPPA2, using default parameters (Trincado *et al.*, 2018). Only events with an adjusted p -val < 0.01 were retained for further analysis. The dPSI (difference in percent spliced in) values for each AS were generated by SUPPA2 and plotted in R using ggplot2. Hypergeometric p -value was calculated using the phyper function in R taking the total number AS event as the population size. Gene ontology enrichment analysis was done using the AgriGO server (<http://bioinfo.cau.edu.cn/agriGO/>) using default parameters. Lists of GO terms were eventually visualized using REVIGO (<http://revigo.irb.hr/>). Gene family enrichment analysis was performed using GenFam (<http://mandadilab.webfactional.com>).

Reverse transcription-quantitative PCR

Total RNA was extracted from plantlets or roots extracted with TriZol (Invitrogen) and subjected (1 μ g of total RNA) to reverse transcription with the Superscript IV reverse transcriptase (Invitrogen). qPCR analyses were performed as described by Nguyen *et al.* (2018). We performed qPCR on triplicate samples of each cDNA from three independent biological replicates. *OXA1* (*At5g62050*) and *UBQ10* (*At4g05320*) were used for the normalization of RT-qPCR data. Quantifications and statistical analyses were performed with SATqPCR (Rancurel *et al.*, 2019), and the results are expressed as normalised relative quantities. For the validation of alternatively spliced genes, two pairs of primers, specifically amplifying one or the two isoforms of the gene concerned, were designed (Table S1) and used for RT-qPCR assays with the parameters described above for the DEG. The *UBQ10* reference gene was used for normalization of the alternatively spliced genes.

Accession numbers

Sequence data from this article can be found in the *Arabidopsis* Information Resource (<https://www.arabidopsis.org/>), Solgenomics (<https://solgenomics.net/>) and GenBank/EMBL databases under the following accession numbers: *Minc18636* (KX907770), *Minc15401* (MT591034), *Minc16401* (MT591035), *AtSmD1a* (At3g07590), *AtSmD1b* (At4g02840), *OXA1* (At5g62050), *UBQ10* (At4g05320), *FAD/NAD(P)-binding oxidoreductase* (At5g11330), *U1 snRNP 70K* (At3g50670), *ribosomal protein S21 family protein* (At3g26360), *RNA-binding (RRM/RBD/RNP motifs)* (At3g04500), *MCM10* (At2g20980), *prenylated RAB acceptor 1.E* (At1g08770), *defensin* (At5g33355), *Solanum lycopersicum SlSmD1a* (Soly06g084310.2.1; MT598822) and *SlSmD1b* (Soly09g064660.2.1; MT598823). The transcriptome data are available at the Sequence Read Archive (SRA) via accession numbers PRJDB5797 (*A. thaliana* galls at 5 and 7 dpi with *M. incognita* and non-inoculated roots; Yamaguchi *et al.*, 2017) and GSE153171 (*A. thaliana* Col-0/P35S:MiEFF18/*smd1b* roots).

Results

MiEFF18 is a secreted effector that localises to the nucleoplasm and nucleolus of plant cells

MiEFF18 is a putative *M. incognita* secreted effector encoded by the *Minc18636* gene. *Minc18636* and its paralog, *Minc15401*, are more strongly expressed at the juvenile parasitic stages than at the J2 pre-parasitic stage, and are specifically expressed in the subventral oesophageal glands (SvG) of both pre-parasitic and parasitic juveniles (Rutter *et al.*, 2014; Nguyen *et al.*, 2018). MiEFF18 displays no similarity to any sequences out of the genus *Meloidogyne* or motifs included in public databases. MiEFF18 is a 312-amino acid (aa) protein with a signal peptide for secretion (aa 1 to 21, according to the Phobius prediction tool (Käll *et al.*, 2007), an N-terminal region rich in aspartic acid and glutamic acid (D-E; 55%) and a C-terminal region enriched in lysine (K; 40%) (Fig. 1a; Fig. S1). *In silico* assays predicted the presence of several nuclear localisation signals (NLS) and one nucleolar localisation signal (NoLS) in MiEFF18 (Fig. 1a), suggesting that this protein would be imported into the nuclei of host plant cells. We produced specific antibodies against the complete MiEFF18 protein in *E. coli*, to check that this protein was, indeed, secreted *in planta*

(Fig. S2a-c). As expected, immunolocalisation experiments on pre-parasitic J2s showed the MiEFF18 to be present in the two SvGs (Fig. 1b-e), consistent with published *in situ* hybridisation results (Rutter *et al.*, 2014; Nguyen *et al.*, 2018). Within the SvGs and their secretory tracks, MiEFF18 localised with punctate structures corresponding to secretory granules (Fig. 1c-e), consistent with its secretion during plant-nematode interactions. No signal was observed, with the exception of a non-specific signal, with the pre-immune serum in pre-parasitic J2s (Fig. S2b-c). To demonstrate secretion of MiEFF18 *in planta*, we used affinity-purified antibodies to immunolocalise MiEFF18 on gall sections (Fig. S2d). MiEFF18 production occurs in the SvGs of parasitic juveniles (Fig. 1f). In galls, we detected MiEFF18 in giant cells where it accumulated in the nuclei (Fig. 1g-h'), confirming its injection within the host cells during *M. incognita* parasitism. No signal was detected within the giant cells when using only the Alexa Fluor 488-conjugated secondary antibody (Fig. S2e-f). These results provide evidence for the secretion of MiEFF18 *in planta* during parasitism and its targeting to the plant cell nucleus.

MiEFF18 interacts with the spliceosomal ribonucleoprotein SmD1

We investigated the effector function of MiEFF18, by performing a yeast two-hybrid (Y2H) screen to search for interactors in tomato. In this system, we used MiEFF18 without its signal peptide as a bait, and a tomato root cDNA library from healthy and *M. incognita*-infected roots (Hybrigenics) as the prey. We screened 48.5 million interactions between MiEFF18 and proteins encoded by the cDNA library. We identified one major target, a ribonucleoprotein, SmD1, which was captured 26 times, whereas other candidates were captured only one to four times (Fig. S3). There are two genes encoding SmD1 proteins with 100% aa identity in *Solanum lycopersicum* (*SlSmD1a_Solyc06g084310* and *SlSmD1b_Solyc09g064660*). Using a pairwise Y2H approach, we independently validated the interaction between the full-length sequences of MiEFF18 and SlSmD1 (*Solyc06g084310*) (Fig. 2a). As a control, we investigated the interaction between SlSmD1 and another *M. incognita* effector, MiEFF16, encoded by the *Minc16401* gene, expressed in the subventral glands, and also localising to the nucleoplasm and the nucleolus of plant cells following transient expression in *Nicotiana benthamiana* leaves (Fig. S4). No interaction was observed between MiEFF16 and SlSmD1 in yeast (Fig. 2a).

We investigated the colocalisation of MiEFF18 and its target, SmD1, in plant cells, by transiently expressing constructs encoding RFP-MiEFF18 and the GFP-SlSmD1 fusion

proteins in *N. benthamiana*. We confirmed the colocalisation of MiEFF18 and SlSmD1 in the nucleoplasm and nucleolus (Fig. 2b). SlSmD1 was also localised in nucleoplasmic speckles, whereas MiEFF18 was not detected in these structures (Fig. 2b). We used a bimolecular fluorescent complementation (BiFC) assay for the validation and localisation *in planta* of the interaction between MiEFF18 and SlSmD1. Using three combinations of BiFC vectors, we showed that MiEFF18 and SlSmD1 interacted strongly in the nucleolus, with a weaker signal observed in the cytoplasm and the nucleoplasm (Fig. 2c and Fig. S5). No interaction was observed between MiEFF16 and SlSmD1, with the various BiFC constructs used (Fig. S5).

Two genes, *AtSmD1a* (*At3g07590*) and *AtSmD1b* (*At4g02840*), encode SmD1 proteins in *A. thaliana*. Using knock-out (KO) mutant lines, Elvira-Matelot et al., (2016) demonstrated that these two genes encode proteins with redundant activities, and that the *smd1a smd1b* double mutant is lethal, as expected for a core component of the spliceosome. The *smd1b* single mutant displays developmental and splicing defects, whereas the *smd1a* single mutant develops normally. *AtSmD1b* would account for a larger proportion of the total activity, probably due to its stronger expression in all tissues compared to *AtSmD1a* (Elvira-Matelot et al., 2016). Using a pairwise Y2H approach, we validated the interaction of the MiEFF18 effector with *AtSmD1a* and *AtSmD1b* (Fig. 2a). Overall, these results demonstrate that the MiEFF18 effector specifically interacts, in yeast and *in planta*, with the tomato and *Arabidopsis* spliceosomal SmD1 core proteins.

MiEFF18 and SmD1 modulate the alternative splicing of plant genes

As MiEFF18 interacts with SmD1, a core component of the spliceosome, we investigated the possible accumulation of similar mis-spliced transcripts in the homozygous *smd1b* mutant and an *Arabidopsis* *MiEFF18*-expressing line, relative to the wild type. We generated transgenic plants expressing the MiEFF18 effector under the control of a 35S promoter (Fig. S6a). Noteworthy, the *MiEFF18*-expressing lines #8.6 and #13.6 exhibited a decreased susceptibility to *M. incognita*, indicating that the continued and excessive presence of MiEFF18 may be detrimental to feeding site formation (Fig. S6b). We performed RNA-sequencing (RNA-seq) on total RNA isolated from the roots of 11-day-old *Arabidopsis* seedlings, Col-0, *smd1b* and *MiEFF18*-expressing line #13.6. Biological triplicates were run for all samples. We then performed transcript quantification with SUPPA2, which is a computational tool that calculate relative inclusion values of alternative splicing events, based of transcript level quantification in RNA-seq data (Trincado et al., 2018; Table S2 and S3).

405 The five main categories of AS events were detected: intron retention (IR), exon skipping
 406 (ES), alternative 5' splice site (A5), alternative 3' splice site (A3) and mutually exclusive
 407 exons (MX) (Fig. 3a; Fig. S7). In total, we identified 249 and 593 differential splicing events,
 408 affecting 222 and 463 genes, in the *MiEFF18*-expressing line and the *smd1b* mutant,
 409 respectively (Fig. 3a-b; Fig. S7). A high degree of overlap was observed between the two
 410 lines, with 113 AS events and 107 alternatively spliced genes common to the two lines
 411 (hypergeometric p value $< 4.666\text{e-}117$; Fig. 3b and Fig. S7). We also compared the dPSI
 412 corresponding to the change in each AS event in both *MiEFF18*-expressing lines and the
 413 *smd1b* mutants (Fig. S8). We found that the global change in AS relative to the wild-type root
 414 was significantly positively correlated in the two lines ($p < 2\text{e-}16$, $R^2 = 0.2406$). We observed an
 415 almost perfect positive correlation if the analysis was restricted to significant differential
 416 splicing events in both lines ($p < 2\text{e-}16$, $R^2 = 0.7613$). The genes concerned belonged to various
 417 families, e.g. the UDP-glucuronate decarboxylase (UXS), the heat shock protein 90 (HSP)
 418 and auxin-responsive (AUX/IAA) gene families (Table S4). The GO analysis however
 419 showed no significant enrichment in any term among the genes displaying AS in the
 420 *MiEFF18*-expressing line or the *smd1b* mutant. Using RT-qPCR, we validated an IR
 421 occurring in the *MiEFF18*-expressing line and the *smd1b* mutant in a the *FAD/NAD(P)-*
 422 *binding oxidoreductase (At5g11330)* gene, and an A3 event in *RNA-binding protein*
 423 *(At3g04500)*, an IR in the *ribosomal protein S21 family protein (At3g26360)* and an A5 event
 424 in *U1 snRNP 70K (At3g50670)* genes occurring in the *smd1b* mutant (Fig. 3e; Fig.S9). Thus,
 425 *MiEFF18* can modulate AS through *SmD1*, as the ectopic expression of *MiEFF18* partially
 426 mimics the global change in AS pattern observed in the *smd1b* mutant line.

427

428 ***M. incognita* triggers alternative splicing during giant cell formation**

429 We used available RNA-seq data from *Arabidopsis* galls at 5 and 7 dpi and from non-
 430 inoculated Col-0 roots (Yamaguchi et al., 2017) to investigate AS events during giant cell
 431 formation in *Arabidopsis*. SUPPA analysis identified 411 and 443 genes that underwent AS in
 432 response to *M. incognita* infection at 5 and 7 dpi, respectively (Fig.3a; Table S5 and S6). In
 433 total, 701 genes were alternatively spliced at either 5 or 7 dpi (Fig. 3c), representing 840
 434 different AS events (Fig. S7d). GO analysis on these 701 AS genes revealed highly significant
 435 enrichment in the term "post embryonic development" ($p\text{-value} = 5.8\text{e-}07$), including 10
 436 *EMBRYO DEFECTIVE (EMB)* genes (*EMB 1353*, *EMB1995/ATS2*, *EMB1629/APO2*, *EMB*
 437 *2728/RPE*, *EMB76/DCL1*, *EMB1006*, *EMB1379*, *EMB2768*, *EMB1401/EIF2 BETA* and

EMB1796/NUWA) and genes involved in hormone signalling (e.g. the gibberellin receptor GA INSENSITIVE DWARF1C, the cytokinin receptor WOODEN LEG (*WOL/CRE1*) and the auxin-responsive IAA28). In addition we noticed an enrichment in GO terms “nucleotide binding” (p -value=2.6e-05), “single-stranded DNA binding” (p -value=5.6e-05) and “ribonucleotide binding” (p -value=5.1e-04) (Table S7). These results provide a first insight into the importance of AS as a regulatory mechanism involved in giant cell formation.

We then investigated whether the modulation of SmD1 function by the MiEFF18 effector could account for the AS observed upon RKN infection. Interestingly, 34.2% (76 genes) and 24.8% (115 genes) of the genes displaying AS changes in the *MiEFF18*-expressing line and in the *smd1b* mutant, respectively, were also affected at 5 or 7 dpi with *M. incognita*; this corresponds to significant enrichment (hypergeometric p -value < 2.0e-61) (Fig. 3d). In total, 39 of the genes displaying AS were common to the three sets of conditions, suggesting that the MiEFF18 effector and SmD1 may be at least partly responsible for the AS occurring in roots in response to RKN infection. These genes included those involved in hormone signalling, such as the auxin-responsive *IAA27*, the *CALCIUM-DEPENDENT PROTEIN KINASE 4 (CPK4)* involved in ABA signalling, and genes encoding RNA-binding proteins, such as *GLYCINE-RICH RNA-BINDING PROTEIN 2 (ATGRP2)* or *NUCLEAR TRANSPORT FACTOR 2 (NTF2)*. Thus MiEFF18 could account for AS triggered in *Arabidopsis* following infection with *M. incognita* to modulate giant cell proteome.

MiEFF18 and SmD1 modulate expression of plant genes involved in giant cell formation

Using RNA-seq data, we also identified 511 and 1,160 differentially expressed genes (DEGs) in the *Arabidopsis* *MiEFF18*-expressing line and the homozygous *smd1b* mutant, respectively, relative to wild-type Col-0 plants (Fig. 4a-c; Table S8 and S9). We found that 187 DEGs (130 upregulated and 57 downregulated genes) were common to *MiEFF18*-expressing and *smd1b* plants. Interestingly, 38.0% of the DEGs in the *MiEFF18*-expressing line and the *smd1b* mutant were also differentially expressed at 5 and/or 7 dpi with *M. incognita* (Fig. 4b-c; Fig. S10; Table S10 and S11). RT-qPCR was used to confirm the RNA-seq data (Fig. 4d). We validated the upregulation of the DNA replication-related *MCM10 (At2g20980)* gene and the downregulation of the *Prenylated RAB acceptor 1.E (At1g08770)* and a defensin (*At5g33355*) genes in the *MiEFF18*-expressing line and/or the *smd1b* mutant, relative to Col-0. These results are consistent with the modulation of plant gene expression by MiEFF18, through interaction with the SmD1 protein. A GO term analysis highlighted an

overrepresentation of genes involved in “microtubule-based movement” (p-value=9.1e-25) and “cell cycle process” (p-value=4.9e-8) in the *MiEFF18*-expressing line, whereas GO terms associated with “plant-type cell wall organization” (p-value=1.1e-05), “response to stimulus” (p-value=4.1e-05) and “response to oxidative stress” (p-value=4.1e-05) were overrepresented in the *smd1b* mutant (Fig. 4e, Fig. S11, Table S7). Interestingly, four GO terms were overrepresented in all three sets of conditions: “cytoskeleton organization”, “cytoskeletal protein binding”, “microtubule binding” and “tubulin binding” (Fig. 4e, Table S7).

***AtSmD1b* is instrumental to root knot nematode parasitism**

We investigated the possible role of Sm proteins, and SmD1 in particular, in RKN parasitism. We began by browsing transcriptomic data to determine whether the expression of *Sm* genes in galls was induced by *M. incognita* infection. Genes encoding the core Sm protein components of the spliceosome, including *AtSmD1a*, are generally induced upon infection (Table S12), suggesting a possible role in the plant-nematode interaction. We investigated the function of *Arabidopsis AtSmD1* genes during parasitism further, by inoculating the *smd1a* and *smd1b Arabidopsis* knockout mutants (Elvira-Matelot et al., 2016) with *M. incognita* J2s. Inoculation resulted in a mean decrease of 30% in the number of females producing egg masses in *smd1b* plants relative to wild-type Col-0 (Fig. 5a). Inoculation had no significant effect on the number of females producing egg masses in *smd1a* plants. This result is consistent with *AtSmD1b* being strongly expressed in *Arabidopsis*, whereas *AtSmD1a* is not (Elvira-Matelot et al., 2016). We investigated whether the giant cells formed on the *smd1b* plants displayed developmental defects. We observed these giant cells directly, under a confocal microscope, after BABB clearing. A comparison of the mean surface areas of the giant cells in each gall showed that giant cells from *smd1b* plants were 37% smaller than those from control plants (Fig. 5b and 5c). Thus, the *AtSmD1b* protein plays an important role in the formation of giant cells and is required for successful nematode infection.

Discussion

MiEFF18 interacts with a nuclear spliceosomal protein

Meloidogyne spp. are among the most devastating plant pathogens, but our understanding of the molecular basis of RKN pathogenicity remains limited. RKN secrete hundreds of effectors, enabling them to overcome host defences and to induce the redifferentiation of root

cells into permanent feeding cells. However, the functions of most of these effectors remain to be determined (Mitchum *et al.*, 2013; Truong *et al.*, 2015; Vieira & Gleason, 2019; Mejias *et al.*, 2019). One of the predicted secreted effectors, MiEFF18, has been shown to be specifically overexpressed within the nematode subventral oesophageal glands at an early stage of parasitism (Rutter *et al.*, 2014; Nguyen *et al.*, 2018).

We showed, by immunolocalisation studies on J2s, that MiEFF18 was present in secretory granules in the subventral gland cells. In plant-parasitic nematodes, these structures are thought to be involved in the delivery of secretions from the oesophageal glands to the stylet, through which they are secreted into the host tissues (Sundermann & Hussey, 1988; Hussey & Mims, 1990; Wang *et al.*, 2010). Immunolocalisation on gall sections further demonstrated MiEFF18 secretion within the giant cells, where it accumulated in the nuclei, validating the *in silico*-predicted nuclear localisation of this effector *in planta*. Secretion has been demonstrated experimentally for very few effectors, and even fewer have been shown to be delivered to the giant cells. *M. incognita* MiMIF-2 (Zhao *et al.*, 2019a) was localised in the cytoplasm, whereas the other effectors (Mi-EFF1, MjNULG1a, MgGPP and Mg16820) were immunolocalised in giant cell nuclei (Jaouannet *et al.*, 2012; Lin *et al.*, 2012; Chen *et al.*, 2017b; Naalden *et al.*, 2018). Our findings support the notion that the nucleus is a key cellular compartment that must be targeted by the parasite, for the regulation of nuclear processes essential for giant cell development, such as cell cycle regulation and transcription (Hewezi & Baum, 2013; Quentin *et al.*, 2013).

Using a Y2H screen, we identified the nuclear spliceosomal SmD1 protein as a potential target of MiEFF18. SmD1, together with six other small ribonucleoprotein particle (Sm) proteins (SmB, SmD2, SmD3, SmE, SmF and SmG), forms a heptameric ring structure surrounding the U-rich small nuclear RNAs (snRNAs) (Matera & Wang, 2014). These snRNP complexes are core components of the spliceosome and play a key role in pre-mRNA splicing (i.e. the correct removal of introns from pre-RNA). When the Sm ring is assembled on the different snRNA molecules in the cytoplasm, it can enter the nucleus, where it initially accumulates in Cajal bodies, and finally, the fully assembled spliceosome executes splicing in the nucleoplasm and, more specifically, in nuclear speckles. Thus, in plants, SmD1 may localise to the nucleoplasm, nucleolus, nuclear speckles, Cajal bodies and cytoplasm, consistent with previous reports (Pendle *et al.*, 2005; Fujioka *et al.*, 2007; Elvira-Matelot *et al.*, 2016; Huertas *et al.*, 2019). We validated the localisation of SmD1 in the cytoplasm and the nucleus, where it could interact with MiEFF18.

537

538 **Ectopic MiEFF18 expression mimics the effect of SmD1 impairment on AS**

539 The finding that the ectopic expression of MiEFF18 *in planta* mimics characteristics of the
 540 *smd1b* mutation provides further evidence in favour of SmD1 being the target of MiEFF18.
 541 AtSmD1b has recently been shown to modulate the AS of specific transcripts (Elvira-Matelot
 542 et al., 2016). In *Arabidopsis*, 70% of the genes may be alternatively spliced, and AS has been
 543 shown to play a significant role in plant development and responses to abiotic stresses (Reddy
 544 et al., 2013; Staiger and Brown, 2013). AS provides a layer of genetic regulation mediating
 545 rapid responses to different stimuli by increasing proteomic diversity. It can affect the
 546 stability of a transcript, particularly if the 5'UTR or 3'UTR is concerned. It can also lead to a
 547 loss/gain of protein function if the open reading frame is modified, by a frameshift or the
 548 creation of a new premature stop codon (Chaudhary et al., 2019). Only a few studies to date
 549 have focused on plant Sm proteins. They investigated the *Arabidopsis* SmD3 (Swaraz et al.,
 550 2011) and SmE (Huertas et al., 2019) proteins, and data are also available for the Sm-Like
 551 protein LSm8, another core component of the spliceosome (Carrasco-López et al., 2017).
 552 Genome-wide AS analysis has confirmed the role of SmE and LSm8 in regulating AS in
 553 *Arabidopsis*, enabling plants to adapt to unfavourable abiotic environments. We expand here,
 554 by a transcriptomic approach, the role of AtSmD1b in regulating AS, and we reveal its crucial
 555 function in a biotic interaction. Our RNAseq data showed that MiEFF18 could coordinate this
 556 AtSmD1b function during RKN parasitism. Indeed, half of the splicing events, in 107 genes,
 557 induced by the ectopic expression of *MiEFF18* in *Arabidopsis*, were also induced by
 558 *AtSmD1b* mutation, suggesting that MiEFF18 controls susceptibility to RKN by directly
 559 modulating the host cell transcriptome.

560

561 **Alternative splicing occurs upon RKN parasitism in *Arabidopsis***

562 AS may play an important role in plant responses to pathogens (Rigo et al., 2019). Very few
 563 studies have reported the AS events occurring in plants in response to infection with bacterial,
 564 viral or fungal pathogens (Howard et al., 2013; Mandadi & Scholthof, 2015; Rubio et al.,
 565 2015; Song et al., 2017; Zheng et al., 2017; Bedre et al., 2019; Ma et al., 2019; Zhang et al.,
 566 2019; Wang et al., 2020). Specific AS events occur in plants in response to a pathogen. A
 567 number of different, specific splice variants have, for example, been shown to accumulate in
 568 wheat in response to infection with two fungal pathogens, *Blumeria graminis* f. sp. *tritici* and
 569 *Puccinia striiformis* f. sp. *tritici* (Zhang et al., 2019). However, the mechanisms regulating the

specificity of the AS of pre-mRNA and controlling stress responses remain poorly understood (Catalá *et al.*, 2019). We provide here a transcriptome-wide description of the AS events occurring in galls 5 and 7 dpi with *M. incognita*. We show that, in galls, AS genes exhibited significant alternative 3' splice site selection rather than intron retention, which is usually predominant in plant response to stress (Laloum *et al.*, 2018). In addition, in galls AS occurs in genes specifically related to giant cell ontogenesis. Indeed, we show enrichment in genes related to post-embryonic organogenesis among the genes displaying AS in galls. The developmental reprogramming required for giant cell formation involves modulation of the expression of genes involved in root cell identity and root development (Yamaguchi *et al.*, 2017; Olmo *et al.*, 2020). The Mi16D10 effector has been shown to manipulate two of these proteins, both of which are SCARECROW-like transcription factors regulating gene expression during root organogenesis (Huang *et al.*, 2006). Our results suggest that MiEFF18, by interfering with AtSmD1b function, may affect these processes in a broader manner, providing transcriptional control over several of these genes.

Recently, effectors have been shown to interfere with the plant spliceosome machinery. The PsAvr3c effector, secreted by the plant pathogenic oomycete *Phytophthora sojae*, has been shown to interfere with the soybean serine/lysine/arginine-rich protein GmSKRP1, modifying the pattern of AS in the host plant to subvert immunity (Huang *et al.*, 2017). Similarly, the *H. schachtii* 30D08 effector has been shown to interact with the *Arabidopsis* SMU2 auxiliary spliceosomal protein. The 30D08 protein allows the cyst nematode to alter pre-mRNA splicing and the expression of genes involved in feeding site development (Verma *et al.*, 2018). We can, thus, hypothesize that, acting through its interaction with a core spliceosomal protein, MiEFF18 modulates the AS occurring in giant cells upon plant-RKN interaction.

MiEFF18 and SmD1 regulate the expression of genes involved in giant cell ontogenesis

A broad reprogramming of transcription occurs upon RKN infection, as already demonstrated in many plants, including *Arabidopsis* (Escobar *et al.*, 2011; Favery *et al.*, 2016; Yamaguchi *et al.*, 2017). Thousands of plant genes involved in diverse processes, including cell cycle activation, cell wall modification, and hormone and defence responses, are differentially expressed during RKN parasitism (Favery *et al.*, 2016). Ectopic expression of *MiEFF18* and partial impairment of SmD1 activity (using the *smd1b* mutant) had similar effects on the expression of various genes differentially expressed upon *M. incognita* infection and giant cell

formation in *Arabidopsis*. In particular, genes involved in DNA replication (e.g. the MCM gene family), in DNA repair and in microtubule network regulation (e.g. encoding kinesins or the MAP65 proteins), or encoding proteins involved in spindle assembly (MAP70-1; IQ DOMAIN 31; TPX2) were upregulated in the *Arabidopsis* lines studied here. This finding is consistent with the synchronised activation of cell cycle processes, such as acytokinetic mitoses and DNA amplification, that occurs during giant cell formation (De Almeida Engler & Gheysen, 2013; Favery *et al.*, 2016). Deregulation of the expression of key regulators of the cell cycle and of cytoskeleton regulators through mutations (e.g. *map65-3* or *wee1.1*), or ectopic expression (e.g. *Kip-Related Protein (KRP)*-expressing lines), leads to defective giant cell development (Caillaud *et al.*, 2008; Coelho *et al.*, 2017; Vieira & de Almeida Engler, 2017; Cabral *et al.*, 2020).

We show here that constitutive expression of the MiEFF18 effector decreases the susceptibility of *Arabidopsis* to *M. incognita*. However, the ectopic expression of MiEFF18 may not reflect what happens under physiological conditions in a giant cell, where the effector must be timely delivered in a precise amount. The excess of some effectors in plants may modify plant physiology and cell function, and confer plant resistance to biotic and/or abiotic stresses. Such observations could be made when expressing *in planta* oomycete effectors (e.g. PsCRN161 or PsCRN115; Rajput *et al.* 2015) or cyst nematode effectors (e.g. Hs32E03 and Hs30D08; Vijayapalani *et al.* 2018 and Verma *et al.* 2018). In addition, the partial impairment of SmD1 function affects the susceptibility of *Arabidopsis* to RKN, impacting giant cell development. Altogether our results demonstrate that MiEFF18 effector interacts with AtSmD1b and may perturbate its homeostasis to facilitate the *de novo* formation of the giant feeding cells unique to RKN parasitism, by regulating key developmental processes.

The answer on how the EFF18 effector manipulates the SmD1 function may come from an analysis of the structure of the MiEFF18. The K-rich C-terminal part of the effector, carrying NLS and NoLS, undoubtedly mediates import into the nucleus, and the N-terminal part of the molecule carries D/E repeats, which are often found in DNA/RNA mimic proteins (Chou & Wang, 2015). These proteins regulate the activity of various DNA/RNA-binding proteins involved in diverse nuclear processes, such as chromatin assembly, DNA repair or transcriptional regulation (Chou & Wang, 2015; Wang *et al.*, 2019). Further studies of this effector-target pair and associated RNAs would improve our understanding of the role and regulation of the spliceosome machinery in plants and might lead to the development of

applications in new control strategies based on the loss of a susceptibility gene essential for development of the disease.

Acknowledgments

We thank Hybrigenics Services (Paris, France) for providing the pB27 and pP6 vectors and the L40ΔGal4 and Y187 yeast strains, and Syngenta for MiEFF18 production. We thank Dr Laurent Deslandes (LIPM, Castanet Tolosan, France) for helpful discussions. Microscopy work was performed at the SPIBOC imaging facility of the Institut Sophia Agrobiotech. We thank Dr Olivier Pierre and the whole platform team for their help with microscopy. We thank Dr Lucie Monticelli for contributing statistical analysis. We thank Dr Janice de Almeida Engler for valuable advice on immunolocalisation. This work was funded by the INRA SPE department and the French Government (National Research Agency, ANR) through the ‘Investments for the Future’ LabEx SIGNALIFE: programme reference #ANR-11-LABX-0028-01, by the INRA-Syngenta Targetome project, by the French-Japanese bilateral collaboration programmes PHC SAKURA 2016 #35891VD and 2019 #43006VJ and by the French-Chinese bilateral collaboration program PHC XU GUANGQI 2020 #45478PF. This work was also supported by the Agence Nationale de la Recherche ANR-16-CE12-0032 (SPLISIL to HV and MC) and the “Laboratoire d’Excellence (LABEX)” Saclay Plant Sciences (SPS; ANR-10-LABX-40). J.M. holds a doctoral fellowship from the French Ministère de l’Enseignement Supérieur, de la Recherche et de l’Innovation (MENRT grant). N.M.T. was supported by a USTH fellowship, as part of the 911-USTH programme of the Ministry of Education and Training of The Socialist Republic of Vietnam. Y.P.C. got scholarships from China Scholarship Council (No. 201806350108) for studying at INRAE, France.

Author contributions

J.M. designed and performed experiments, and interpreted results; J.M., Y.P.C. and N.M.T. performed yeast two-hybrid assays and generated constructs; SW, J.B. and M.D.C. performed the transcriptome analysis and analysed AS data; H.V. and N.B. contributed material and analysed the data; N.M. produced the nematodes and tomato plants; J.M., J.B., H.V., P.A., B.F. and M.Q. wrote the article; P.A., B.F. and M.Q. obtained funding, designed the work and supervised the experiments and data analyses; all the authors read and edited the article.

References

- de Almeida Engler J, Favery B. 2011.** The Plant Cytoskeleton Remodelling in Nematode Induced Feeding Sites. In: *Genomics and Molecular Genetics of Plant-Nematode Interactions*. Dordrecht: Springer Netherlands, 369–393.
- de Almeida Engler J, Gheysen G. 2013.** Nematode-induced endoreduplication in plant host cells: why and how? *Molecular Plant-Microbe Interactions* **26**: 17–24.
- Barnes SN, Wram CL, Mitchum MG, Baum TJ. 2018.** The plant-parasitic cyst nematode effector GLAND4 is a DNA-binding protein. *Molecular Plant Pathology* **19**: 2263–2276.
- Bartlem DG, Jones MGKK, Hammes UZ. 2014.** Vascularization and nutrient delivery at root-knot nematode feeding sites in host roots. *Journal of Experimental Botany* **65**: 1789–1798.
- Bedre R, Irigoyen S, Schaker PDC, Monteiro-Vitorello CB, Da Silva JA, Mandadi KK. 2019.** Genome-wide alternative splicing landscapes modulated by biotrophic sugarcane smut pathogen. *Scientific Reports* **9**: 1–12.
- Bent AF, Clough SJ. 1998.** Agrobacterium Germ-Line Transformation: Transformation of Arabidopsis without Tissue Culture. In: *Plant Molecular Biology Manual*. Springer Netherlands, 17–30.
- Cabral D, Banora MY, Antonino JD, Rodiuc N, Vieira P, Coelho RR, Chevalier C, Eekhout T, Engler G, De Veylder L, *et al.* 2020.** The plant WEE1 kinase is involved in checkpoint control activation in nematode-induced galls. *New Phytologist* **225**: 430–447.
- Cabrera J, Bustos R, Favery B, Fenoll C, Escobar C. 2014.** NEMATIC: A simple and versatile tool for the insilico analysis of plant-nematode interactions. *Molecular Plant Pathology* **15**: 627–636.
- Cabrera J, Olmo R, Ruiz-Ferrer V, Abreu I, Hermans C, Martinez-Argudo I, Fenoll C, Escobar C. 2018.** A Phenotyping Method of Giant Cells from Root-Knot Nematode Feeding Sites by Confocal Microscopy Highlights a Role for CHITINASE-LIKE 1 in Arabidopsis. *International Journal of Molecular Sciences* **19**: 429.
- Caillaud M-C, Abad P, Favery B. 2008.** Cytoskeleton reorganization. *Plant Signaling & Behavior* **3**: 816–818.
- Caillaud M-C, Favery B. 2016.** In Vivo Imaging of Microtubule Organization in Dividing Giant Cell. In: Caillaud M-C, ed. *Methods in Molecular Biology*. New York: Springer New York, 137–144.
- Caillaud M-C, Paganelli L, Lecomte P, Deslandes L, Quentin M, Pecrix Y, Le Bris M,**

- 701 **Marfaing N, Abad P, Favery B. 2009.** Spindle Assembly Checkpoint Protein Dynamics
 702 Reveal Conserved and Unsuspected Roles in Plant Cell Division. *PLoS ONE* **4**: e6757.
- 703 **Carrasco-López C, Hernández-Verdeja T, Perea-Resa C, Abia D, Catalá R, Salinas J.**
 704 **2017.** Environment-dependent regulation of spliceosome activity by the LSM2-8 complex in
 705 Arabidopsis. *Nucleic Acids Research* **45**: 7416–7431.
- 706 **Catalá R, Carrasco-López C, Perea-Resa C, Hernández-Verdeja T, Salinas J. 2019.**
 707 Emerging roles of lsm complexes in posttranscriptional regulation of plant response to abiotic
 708 stress. *Frontiers in Plant Science* **10**: 167.
- 709 **Chaudhary S, Khokhar W, Jabre I, Reddy ASN, Byrne LJ, Wilson CM, Syed NH. 2019.**
 710 Alternative splicing and protein diversity: Plants versus animals. *Frontiers in Plant Science*
 711 **10**: 708.
- 712 **Chen J, Lin B, Huang Q, Hu L, Zhuo K, Liao J. 2017.** A novel Meloidogyne graminicola
 713 effector, MgGPP, is secreted into host cells and undergoes glycosylation in concert with
 714 proteolysis to suppress plant defenses and promote parasitism. *PLoS Pathogens* **13**:
 715 e1006301.
- 716 **Chou CC, Wang AHJ. 2015.** Structural D/E-rich repeats play multiple roles especially in
 717 gene regulation through DNA/RNA mimicry. *Molecular BioSystems* **11**: 2144–2151.
- 718 **Coelho RR, Vieira P, Antonino de Souza Júnior JD, Martin-Jimenez C, De Veylder L,**
 719 **Cazareth J, Engler G, Grossi-de-Sa MF, de Almeida Engler J. 2017.** Exploiting cell cycle
 720 inhibitor genes of the KRP family to control root-knot nematode induced feeding sites in
 721 plants. *Plant Cell and Environment* **40**: 1174–1188.
- 722 **Deslandes L, Rivas S. 2011.** The plant cell nucleus. *Plant Signaling & Behavior* **6**: 42–48.
- 723 **Elvira-Matlot E, Bardou F, Ariel F, Jauvion V, Bouteiller N, Le Masson I, Cao J,**
 724 **Crespi MD, Vaucheret H. 2016.** The Nuclear Ribonucleoprotein SmD1 Interplays with
 725 Splicing, RNA Quality Control, and Posttranscriptional Gene Silencing in Arabidopsis. *The*
 726 *Plant Cell* **28**: 426–438.
- 727 **Escobar C, Brown S, Mitchum M. 2011.** Transcriptomic and Proteomic Analysis of the
 728 Plant response to Nematode Infection. In: Jones J, Gheysen G, Fenoll C, eds. Genomics and
 729 Molecular Genetics of Plant-Nematode Interactions. Dordrecht, Heidelberg, London & New
 730 York: Springer, 157–173.
- 731 **Favery B, Quentin M, Jaubert-Possamai S, Abad P. 2016.** Gall-forming root-knot
 732 nematodes hijack key plant cellular functions to induce multinucleate and hypertrophied
 733 feeding cells. *Journal of Insect Physiology*. **84**: 60-69.

- 734 **Fujioka Y, Utsumi M, Ohba Y, Watanabe Y. 2007.** Location of a possible miRNA
735 processing site in SmD3/SmB nuclear bodies in arabidopsis. *Plant and Cell Physiology* **48**:
736 1243–1253.
- 737 **Hewezi T, Baum TJ. 2013.** Manipulation of Plant Cells by Cyst and Root-Knot Nematode
738 Effectors. *Molecular Plant-Microbe Interactions* **26**: 9–16.
- 739 **Howard BE, Hu Q, Babaoglu AC, Chandra M, Borghi M, Tan X, He L, Winter-Sederoff**
740 **H, Gassmann W, Veronese P, et al. 2013.** High-Throughput RNA Sequencing of
741 Pseudomonas-Infected Arabidopsis Reveals Hidden Transcriptome Complexity and Novel
742 Splice Variants. *PLoS ONE* **8**: e74183.
- 743 **Huang GZ, Allen R, Davis EL, Baum TJ, Hussey RS. 2006a.** Engineering broad root-knot
744 resistance in transgenic plants by RNAi silencing of a conserved and essential root-knot
745 nematode parasitism gene. *Proceedings of the National Academy of Sciences of the United*
746 *States of America* **103**: 14302–14306.
- 747 **Huang G, Dong R, Allen R, Davis EL, Baum TJ, Hussey RS. 2006b.** A Root-Knot
748 Nematode Secretory Peptide Functions as a Ligand for a Plant Transcription Factor. *Mol*
749 *Plant Microbe Interact* **19**: 463–470.
- 750 **Huang J, Gu L, Zhang Y, Yan T, Kong G, Kong L, Guo B, Qiu M, Wang Y, Jing M, et**
751 **al. 2017.** An oomycete plant pathogen reprograms host pre-mRNA splicing to subvert
752 immunity. *Nature Communications* **8**: 2051.
- 753 **Huertas R, Catalá R, Jiménez-Gómez JM, Castellano MM, Crevillén P, Piñeiro M,**
754 **Jarillo JA, Salinas J. 2019.** Arabidopsis SME1 regulates plant development and response to
755 abiotic stress by determining spliceosome activity Specificity. *Plant Cell* **31**: 537–554.
- 756 **Hussey RS, Mims CW. 1990.** Ultrastructure of esophageal glands and their secretory
757 granules in the root-knot nematode *Meloidogyne incognita*. *Protoplasma* **165**: 9–18.
- 758 **Jaouannet M, Perfus-Barbeoch L, Deleury E, Magliano M, Engler G, Vieira P, Danchin**
759 **EGJ, Rocha M Da, Coquillard P, Abad P, et al. 2012.** A root-knot nematode-secreted
760 protein is injected into giant cells and targeted to the nuclei. *New Phytologist* **194**: 924–931.
- 761 **Jaubert-Possamai S, Noureddine Y, Favery B. 2019.** MicroRNAs, New Players in the
762 Plant–Nematode Interaction. *Frontiers in Plant Science* **10**: 1180.
- 763 **Jaubert S, Milac AL, Petrescu AJ, de Almeida-Engler J, Abad P, Rosso M-N. 2005.** In
764 Planta Secretion of a Calreticulin by Migratory and Sedentary Stages of Root-Knot
765 Nematode. *Molecular Plant-Microbe Interactions* **18**: 1277–1284.
- 766 **Käll L, Krogh A, Sonnhammer ELL. 2007.** Advantages of combined transmembrane

- topology and signal peptide prediction-the Phobius web server. *Nucleic Acids Research* **35**: 429–432.
- Karimi M, Depicker A, Hilson P. 2007.** Recombinational cloning with plant gateway vectors. *Plant Physiology* **145**: 1144–1154.
- Laloum T, Martín G, Duque P. 2018.** Alternative Splicing Control of Abiotic Stress Responses. *Trends in Plant Science* **23**: 140–150.
- Lin B, Zhuo K, Wu P, Cui R, Zhang L-H, Liao J. 2012.** A Novel Effector Protein, MJ-NULG1a, Targeted to Giant Cell Nuclei Plays a Role in *Meloidogyne javanica* Parasitism. *Molecular Plant-Microbe Interactions* **26**: 55–66.
- Ma JQ, Wie LJ, Lin A, Zhang C, Sun W, Yang B, Lu K, Li JN. 2019.** The alternative splicing landscape of brassica napus infected with *leptosphaeria maculans*. *Genes* **10**: 296.
- Mandadi KK, Scholthof KBG. 2015.** Genome-wide analysis of alternative splicing landscapes modulated during plant-virus interactions in *brachypodium distachyon*. *Plant Cell* **27**: 71–85.
- Matera AG, Wang Z. 2014.** Erratum: A day in the life of the spliceosome (Nature Reviews Molecular Cell Biology (2014) 15 (108-122)). *Nature Reviews Molecular Cell Biology* **15**: 294.
- Mejias J, Truong NM, Abad P, Favery B, Quentin M. 2019.** Plant Proteins and Processes Targeted by Parasitic Nematode Effectors. *Frontiers in Plant Science* **10**: 970.
- Mitchell A, Chang HY, Daugherty L, Fraser M, Hunter S, Lopez R, McAnulla C, McMenamin C, Nuka G, Pesseat S, et al. 2015.** The InterPro protein families database: The classification resource after 15 years. *Nucleic Acids Research* **43**: D213-D221.
- Mitchum MG, Hussey RS, Baum TJ, Wang X, Elling AA, Wubben M, Davis EL. 2013.** Nematode effector proteins: An emerging paradigm of parasitism. *New Phytologist* **199**: 879–894.
- Motion GB, Amaro TMMM, Kulagina N, Huitema E. 2015.** Nuclear processes associated with plant immunity and pathogen susceptibility. *Briefings in Functional Genomics* **14**: 243–252.
- Naalden D, Haegeman A, de Almeida-Engler J, Birhane Eshetu F, Bauters L, Gheysen G. 2018.** The *Meloidogyne graminicola* effector Mg16820 is secreted in the apoplast and cytoplasm to suppress plant host defense responses. *Molecular Plant Pathology* **19**: 2416–2430.
- Nguyen C-N, Perfus-Barbeoch L, Quentin M, Zhao J, Magliano M, Marteu N, Da Rocha**

- 800 **M, Nottet N, Abad P, Favery B. 2018.** A root-knot nematode small glycine and cysteine-rich
 801 secreted effector, MiSGCR1, is involved in plant parasitism. *New Phytologist* **217**: 687–699.
- 802 **Olmo R, Cabrera J, Díaz-Manzano FE, Ruiz-Ferrer V, Barcala M, Ishida T, García A,**
 803 **Andrés MF, Ruiz-Lara S, Verdugo I, et al. 2020.** Root-knot nematodes induce gall
 804 formation by recruiting developmental pathways of post-embryonic organogenesis and
 805 regeneration to promote transient pluripotency. *New Phytologist* **227**: 200–215.
- 806 **Pendle AF, Clark GP, Boon R, Lewandowska D, Lam YW, Andersen J, Mann M,**
 807 **Lamond AI, Brown JWS, Shaw PJ. 2005.** Proteomic Analysis of the Arabidopsis Nucleolus
 808 Suggests Novel Nucleolar Functions □ D. *Molecular Biology of the Cell* **16**: 260–269.
- 809 **Postnikova OA, Hult M, Shao J, Skantar A, Nemchinov LG. 2015.** Transcriptome analysis
 810 of resistant and susceptible alfalfa cultivars infected with root-knot nematode *Meloidogyne*
 811 *incognita*. *PloS one*. 10(3): e0123157.
- 812 **Quentin M, Abad P, Favery B. 2013.** Plant parasitic nematode effectors target host defense
 813 and nuclear functions to establish feeding cells. *Frontiers in Plant Science* **4**: 53.
- 814 **Rancurel C, van Tran T, Elie C, Hilliou F. 2019.** SATQPCR: Website for statistical
 815 analysis of real-time quantitative PCR data. *Molecular and Cellular Probes* **46**: 101418.
- 816 **Reddy ASN, Marquez Y, Kalyna M, Barta A. 2013.** Complexity of the Alternative Splicing
 817 Landscape in Plants. *The Plant Cell* **25**: 3657–3683.
- 818 **Rigo R, Bazin J, Crespi M, Charon C. 2019.** Alternative Splicing in the Regulation of
 819 Plant-Microbe Interactions. *Plant and Cell Physiology* **60**: 1906–1916.
- 820 **Rubio M, Rodríguez-Moreno L, Ballester AR, de Moura MC, Bonghi C, Candresse T,**
 821 **Martínez-Gómez P. 2015.** Analysis of gene expression changes in peach leaves in response
 822 to Plum pox virus infection using RNA-Seq. *Molecular Plant Pathology* **16**: 164–176.
- 823 **Rutter WB, Hewezi T, Abubucker S, Maier TR, Huang G, Mitreva M, Hussey RS,**
 824 **Baum TJ. 2014.** Mining Novel Effector Proteins from the Esophageal Gland Cells of
 825 *Meloidogyne incognita*. *Molecular plant-microbe interactions* **27**: 965–974.
- 826 **Shukla N, Yadav R, Kaur P, Rasmussen S, Goel S, Agarwal M, Jagannath A, Gupta R,**
 827 **Kumar A. 2018.** Transcriptome analysis of root-knot nematode (*Meloidogyne incognita*)-
 828 infected tomato (*Solanum lycopersicum*) roots reveals complex gene expression profiles and
 829 metabolic networks of both host and nematode during susceptible and resistance responses.
 830 *Molecular Plant Pathology* **19**: 615–633.
- 831 **Singh SK, Hodda M, Ash GJ. 2013.** Plant-parasitic nematodes of potential phytosanitary
 832 importance, their main hosts and reported yield losses. *EPPO Bulletin* **43**: 334–374.

- 833 **Song J, Liu H, Zhuang H, Zhao C, Xu Y, Wu S, Qi J, Li J, Hettenhausen C, Wu J. 2017.**
 834 Transcriptomics and Alternative Splicing Analyses Reveal Large Differences between Maize
 835 Lines B73 and Mo17 in Response to Aphid *Rhopalosiphum padi* Infestation. *Frontiers in*
 836 *Plant Science* **8**: 1738.
- 837 **Staiger D, Brown JWS. 2013.** Alternative splicing at the intersection of biological timing,
 838 development, and stress responses. *Plant Cell* **25**: 3640–3656.
- 839 **Sundermann CA, Hussey RS. 1988.** Ultrastructural Cytochemistry of Secretory Granules of
 840 Esophageal Glands of *Meloidogyne incognita*. *Journal of nematology* **20**: 141–149.
- 841 **Swaraz AM, Park YD, Hur Y. 2011.** Knock-out mutations of Arabidopsis SmD3-b induce
 842 pleiotropic phenotypes through altered transcript splicing. *Plant Science* **180**: 661–671.
- 843 **Trincado JL, Entizne JC, Hysenaj G, Singh B, Skalic M, Elliott DJ, Eyraas E. 2018.**
 844 SUPPA2: Fast, accurate, and uncertainty-aware differential splicing analysis across multiple
 845 conditions. *Genome Biology* **19**: 40.
- 846 **Truong NM, Nguyen C-N, Abad P, Quentin M, Favery B. 2015.** Function of Root-Knot
 847 Nematode Effectors and Their Targets in Plant Parasitism. In: Escobar C, Fenoll C, eds.
 848 Advance in Botanical Research: Plant Nematode Interactions A View on Compatible
 849 Interrelationships. Academic Press, 293–324.
- 850 **Verma A, Lee C, Morriss S, Odu F, Kenning C, Rizzo N, Spollen WG, Lin M, McRae**
 851 **AG, Givan SA, et al. 2018.** The novel cyst nematode effector protein 30D08 targets host
 852 nuclear functions to alter gene expression in feeding sites. *New Phytologist* **219**: 697–713.
- 853 **Vieira P, de Almeida Engler J. 2017.** Plant cyclin-dependent kinase inhibitors of the KRP
 854 family: Potent inhibitors of root-knot nematode feeding sites in plant roots. *Frontiers in Plant*
 855 *Science* **8**: 1514.
- 856 **Vieira P, Gleason C. 2019.** Plant-parasitic nematode effectors — insights into their diversity
 857 and new tools for their identification. *Current Opinion in Plant Biology* **50**: 37–43.
- 858 **Vijayapalani P, Hewezi T, Pontvianne F, Baum TJ. 2018.** An Effector from the Cyst
 859 Nematode *Heterodera schachtii* Derepresses Host rRNA Genes by Altering Histone
 860 Acetylation. *The Plant Cell* **30**: tpc.00570.2018.
- 861 **Wang L, Chen M, Zhu F, Fan T, Zhang J, Lo C. 2020.** Alternative splicing is a Sorghum
 862 bicolor defense response to fungal infection. *Planta* **251**: 1–13.
- 863 **Wang HC, Chou CC, Hsu KC, Lee CH, Wang AHJ. 2019.** New paradigm of functional
 864 regulation by DNA mimic proteins: Recent updates. *IUBMB Life* **71**: 539–548.
- 865 **Wang J, Lee C, Replogle A, Joshi S, Korkin D, Hussey R, Baum TJ, Davis EL, Wang X,**

- 866 **Mitchum MG. 2010.** Dual roles for the variable domain in protein trafficking and host-
 867 specific recognition of Heterodera glycines CLE effector proteins. *New Phytologist* **187**:
 868 1003–1017.
- 869 **Wilkinson ME, Charenton C. 2020.** RNA Splicing by the Spliceosome. *Annual Review of*
 870 *Biochemistry* **89**: 359-388.
- 871 **Yamaguchi YL, Suzuki R, Cabrera J, Nakagami S, Sagara T, Ejima C, Sano R, Aoki Y,**
 872 **Olmo R, Kurata T, et al. 2017.** Root-Knot and Cyst Nematodes Activate Procambium-
 873 Associated Genes in Arabidopsis Roots. *Frontiers in Plant Science* **8**: 1195.
- 874 **Zhang L, Davies LJ, Elling A a. 2014.** A *Meloidogyne incognita* effector is imported into
 875 the nucleus and exhibits transcriptional activation activity *in planta*. *Molecular plant*
 876 *pathology* **16**(1): 48-60.
- 877 **Zhang H, Mao R, Wang Y, Zhang L, Wang C, Lv S, Liu X, Wang Y, Ji W. 2019.**
 878 Transcriptome-wide alternative splicing modulation during plant-pathogen interactions in
 879 wheat. *Plant Science* **288**: 110160.
- 880 **Zhao J, Li L, Liu Q, Liu P, Li S, Yang D, Chen Y, Pagnotta S, Favery B, Abad P, et al.**
 881 **2019.** A MIF-like effector suppresses plant immunity and facilitates nematode parasitism by
 882 interacting with plant annexins. *Journal of Experimental Botany* **70**: 5943–5958.
- 883 **Zheng Y, Wang Y, Ding B, Fei Z. 2017.** Comprehensive Transcriptome Analyses Reveal
 884 that Potato Spindle Tuber Viroid Triggers Genome-Wide Changes in Alternative Splicing,
 885 Inducible trans- Acting Activity of Phased Secondary Small Interfering RNAs, and Immune
 886 Responses Yi. **91**: e002447-17.
- 887

Figure legends

Fig. 1 MiEFF18 is a secreted effector that localises to the nucleus and nucleolus of plant cells. (a) Schematic diagram of the MiEFF18 protein. The predicted secretion signal peptide (SP; red box), the aspartic acid and glutamic acid (D-E)-rich region (purple box), the lysine (K)-rich C-terminal region (yellow box), nuclear localisation signals (NLS) and the nucleolar localisation signal (NoLS) are shown. The NLS pat4 (KKPK, aa 235-238) and pat 7 (PAKKGKK, aa 292-298) are indicated in grey and the bipartite region (KGA AKVAKKDTKKPKD, aa 223-239) is shown in black. (b) Schematic diagram of a section through a J2. (c-e) Immunolocalisation of MiEFF18 in the subventral glands (SvGs) of *M. incognita* pre-parasitic J2s. (f) Immunolocalisation of MiEFF18 in the subventral glands (SvGs) of parasitic *M. incognita*. Confocal images of J2s treated with rabbit anti-MiEFF18 serum and goat anti-rabbit Alexa Fluor 488 secondary antibodies are shown. Fluorescence signals are visible in the secretory granules of the subventral glands (magnification in the insets) and in the secretory tracts (arrow). Corresponding bright-field images of the juveniles are shown in the left. Bars = 10 µm. m, metacarpus, n, nucleus, SvGs, subventral glands. (g-h') Localization of the secreted MiEFF18 protein in plant tissues. MiEFF18 accumulated in the giant cell nuclei. Images of Alexa Fluor 488 fluorescence, DAPI-stained nuclei and overlays are shown. (h') is an enlargement of the area framed in (h). *, giant cell. Bars = 10 µm.

Fig. 2 The MiEFF18 effector interacts with SmD1 proteins in the nucleus and nucleolus of plant cells. (a) Diploid yeasts containing the bait and prey plasmids carrying controls, effectors or SmD1 proteins (*Solanum lycopersicum* SlSmD1 and *Arabidopsis thaliana*, AtSmD1a and AtSmD1b) were spotted on plates. SD-WL corresponds to the non-selective medium without tryptophan (W) and leucine (L). Only yeasts carrying a protein-protein interaction can survive on the SD-WLH (H, histidine) + 0.5 mM 3-AT selective medium. Murine p53 and SV40 T-antigen T (anti T) were used as a positive control, and MiEFF16 was used as a negative control. (b) Colocalisation of RFP-MiEFF18 and GFP-SlSmD1 in *N. benthamiana* epidermal leaf cells. RFP and GFP were used as a nucleocytoplasmic control. Bars = 5µm. (c) MiEFF18 and SlSmD1 interact together in the nucleolus, nucleoplasm and cytoplasm in *N. benthamiana* cells. YFP fluorescence confocal images of bimolecular fluorescence complementation (BiFC) experiments with different combinations of YFPc or

922 YFNn fused, at the C- or N-terminus, to SlSmD1 and MiEFF18, expressed in *N. benthamiana*
 923 epidermal cells. The MiEFF16 effector was used as a negative control. Bars = 10 μ m.

924

925 **Fig. 3** SmD1b modulates alternative splicing in *Arabidopsis* roots. (a) *Arabidopsis* genes with
 926 alternative splicing (AS) events (intron retention, exon skipping, alternative 5' splice site,
 927 alternative 3' splice site, mutually exclusive exons) in the *MiEFF18*-expressing line and the
 928 *smd1b* mutant, relative to Col-0 roots, and in galls five and seven days post inoculation (dpi)
 929 with *M. incognita*, relative to uninfected *Arabidopsis* Col-0 roots. (b) Venn diagram showing
 930 the overlap between alternatively spliced genes in the *MiEFF18*-expressing line and *smd1b*
 931 mutant plants. (c) Venn diagram showing the overlap between alternatively spliced genes in
 932 *M. incognita*-induced galls at 5 and 7 dpi. (d) Venn diagram showing the overlap between
 933 genes affected in the *MiEFF18*-expressing line, *smd1b* mutant and in *M. incognita*-induced
 934 galls at 5 or 7 dpi. (e) Validation of the changes in AS pattern detected in the roots of
 935 *Arabidopsis* *MiEFF18*-expressing line, *smd1b* mutant and wild-type Col-0 by RT-qPCR. Data
 936 were normalised using *UBQ10* as a reference gene. Asterisks indicate significant differences
 937 (**P < 0.001, ***P < 0.0001) compared to wild-type plants, as determined by t-student test
 938 (SatqPCR software). Error bars indicate the SE. Left panels show the part of the alternately
 939 spliced genes (the black boxes represent the exons, the lines represent the introns) and the
 940 read mapping of the RNAseq (y-axis).

941

942 **Fig. 4** MiEFF18 and SMD1b regulate transcript accumulation in *Arabidopsis* root. (a)
 943 Quantification of differentially expressed genes (DEG) in the roots of the *MiEFF18*-
 944 expressing *Arabidopsis* line (EFF18) and the *smd1b* mutant, relative to Col-0 roots. The
 945 overlap between genes differentially expressed (up: induced; down: repressed) in the EFF18
 946 line and the *smd1b* mutant is shown. (b) Venn diagram showing the overlaps between genes
 947 induced (up) in the *MiEFF18*-expressing line, the *smd1b* mutant and in *M. incognita*-induced
 948 galls at 5 or 7 dpi. (c) Venn diagram showing the overlaps between genes repressed (down) in
 949 the *MiEFF18*-expressing line, the *smd1b* mutant and in *M. incognita*-induced galls at 5 or
 950 7dpi. (d) Validation of the expression of DEG identified in the *smd1b* mutant and/or the
 951 *MiEFF18*-expressing line, by RT-qPCR. Data were normalized against *UBQ10* and *OXA1* as
 952 constitutive genes. Asterisks indicate significant differences (*P < 0.01) between *MiEFF18*-
 953 expressing line or the *smd1b* mutants compared to wild-type (Col-0) plants, as determined by
 954 t-student test (SatqPCR software). Error bars indicate the SE. (e) Enrichment in GO terms for

biological processes among DEGs in the *MiEFF18*-expressing line, *smd1b* mutant and in galls five and seven days after inoculation with *M. incognita*. Only GO terms displaying statistically significant enrichment (FDR<0.05) in at least two sets of conditions are presented.

Fig. 5 AtSmD1b is instrumental to root-knot nematode parasitism. (a) Box-and-whisker plots of females producing egg masses per plant in Col-0 control line, *smd1a*, *smd1b* lines six weeks post infection with 200 *M. incognita* J2s. The three independent experiments are presented. The effect of plant genotype on the number of nematode egg masses was analyzed with generalized linear models (GLMs) based on a Poisson distribution, for each replicate. We used the Tukey adjustment method ('multcomp' package) for multiple testing. Different letters indicate statistically significant difference between each column. (b) Galls of Col-0 and *smd1b* plants collected two weeks post infection to measure the surface of the giant cells (dotted line) using BABB clearing method (Cabrera et al., 2018). (c) Box-and-whisker plot of giant cell size (μm^2) measures on Col-0 and *smd1b* plants. The impact of the plant genotype on the surface of giant cells was analysed using student t test. Combined data from two independent biological replicates are shown (n=42 and n=25). Significance of terms: ***P < 0.001.

Supporting information

Table S1 Primers used in this study.

Table S2 Altered splicing events identified in the *Arabidopsis* MiEFF18-expressing line

Table S3 Altered splicing events identified in the *Arabidopsis* *smd1b* mutant line.

Table S4 Gene family (GenFam) enrichment analyses.

Table S5 Altered splicing events identified in *Arabidopsis thaliana* at 5 dpi with *Meloidogyne incognita*.

Table S6 Altered splicing events identified in *Arabidopsis thaliana* at 7 dpi with *Meloidogyne incognita*.

Table S7 Gene Ontology (GO) analyses.

Table S8 Differentially expressed genes identified in the *Arabidopsis* MiEFF18-expressing line

Table S9 Differentially expressed genes identified in the *Arabidopsis* *smd1b* mutant line.

985 **Table S10** Differentially expressed genes identified in *Arabidopsis thaliana* at 5 dpi with
 986 *Meloidogyne incognita*.

987 **Table S11** Differentially expressed genes identified in *Arabidopsis thaliana* at 7 dpi with
 988 *Meloidogyne incognita*.

989 **Table S12** Expression of the different *Arabidopsis* small nuclear ribonucleoprotein Sm core
 990 genes during *M. incognita* infection.

991

992 **Fig. S1** Alignment of the Minc18636 and Minc15401 proteins.

993 **Fig. S2** Specificity of the α -MiEFF18 and pre-immune serums.

994 **Fig. S3** Results of the yeast two-hybrid screen using MiEFF18 as a bait against the tomato
 995 root cDNA library.

996 **Fig. S4** Minc16401 encodes a putative effector targeting the plant cell nucleus and nucleoli.

997 **Fig. S5** Bimolecular fluorescence complementation (BiFC) experiments in *N. benthamiana*
 998 cells showed that SLSmD1 interact with MiEFF18, but not with MiEFF16.

999 **Fig. S6** *MiEFF18*-expression in *Arabidopsis* transgenic lines altered *M. incognita*
 1000 reproduction.

1001 **Fig. S7** MiEFF18 and SmD1b modulate alternative splicing in *Arabidopsis* roots.

1002 **Fig. S8** Effect of *MiEFF18* expression and *smd1b* mutation on AS are positively correlated.

1003 **Fig. S9** Example of alternative splicing qPCR validation for the U1-70K mRNA isoform.

1004 **Fig. S10** Venn diagrams of differentially expressed genes (DEG) in roots of the MiEFF18-
 1005 expressing line, the *smd1b* mutant and in *M. incognita*-induced galls at 5 or 7dpi.

1006 **Fig. S11** Gene ontology (GO)-term enrichment of differentially expressed genes (DEG) in the
 1007 *MiEFF18*-expressing line and the *smd1b* mutant.

1008

1009

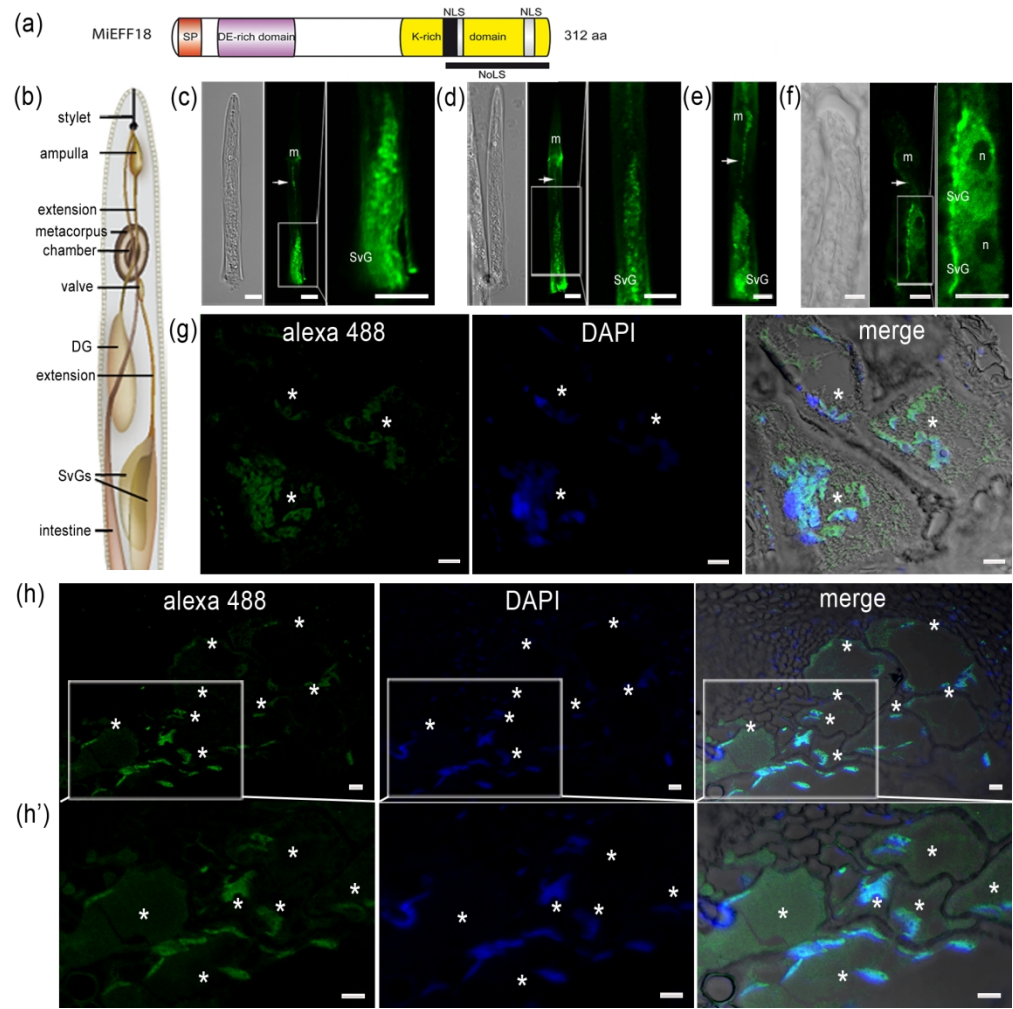


Figure 1

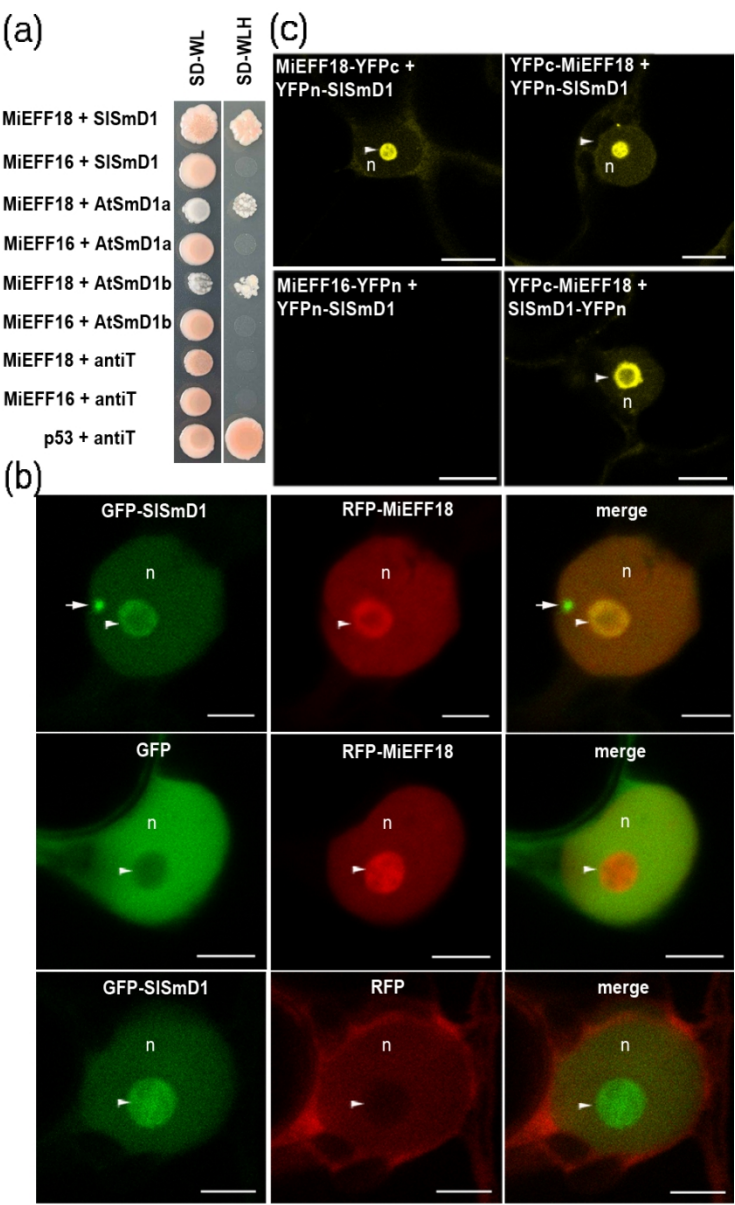


Figure 2

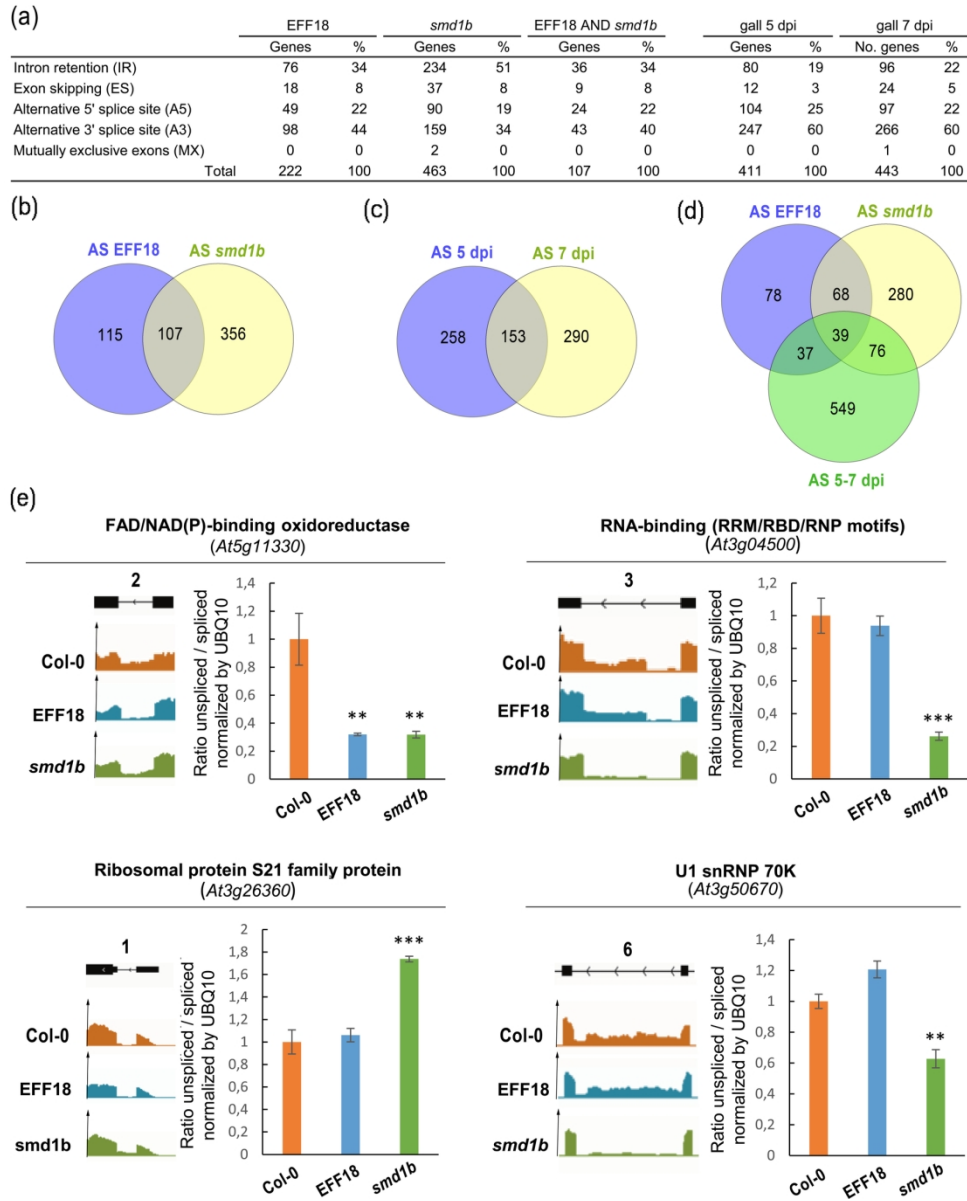


Figure 3

160x195mm (300 x 300 DPI)

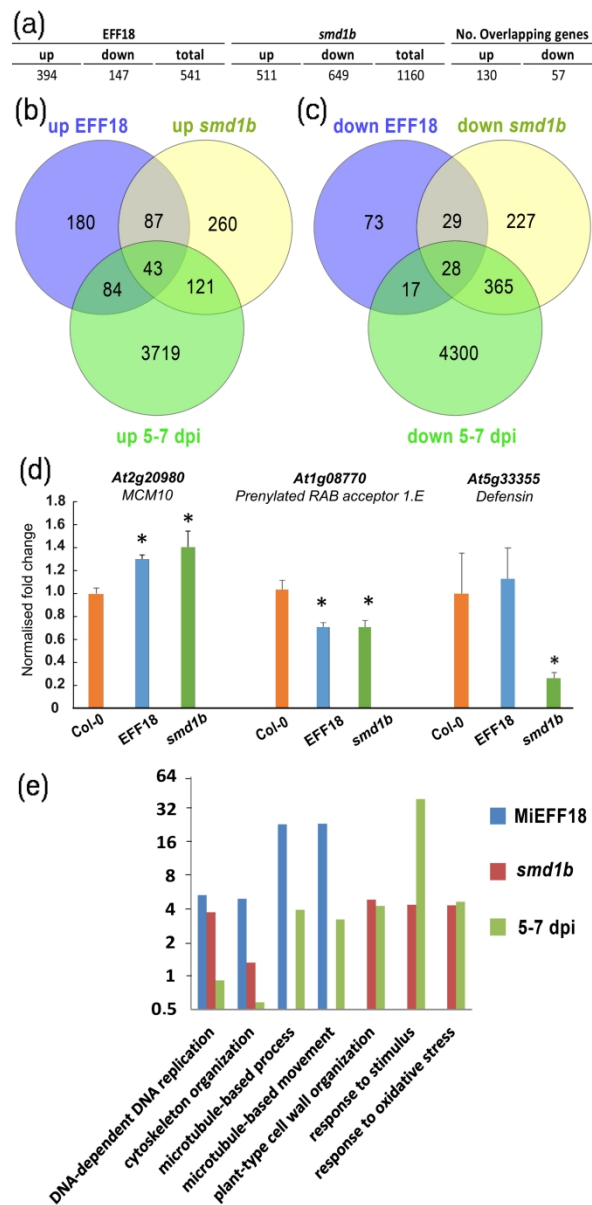


Figure 4

80x164mm (600 x 600 DPI)

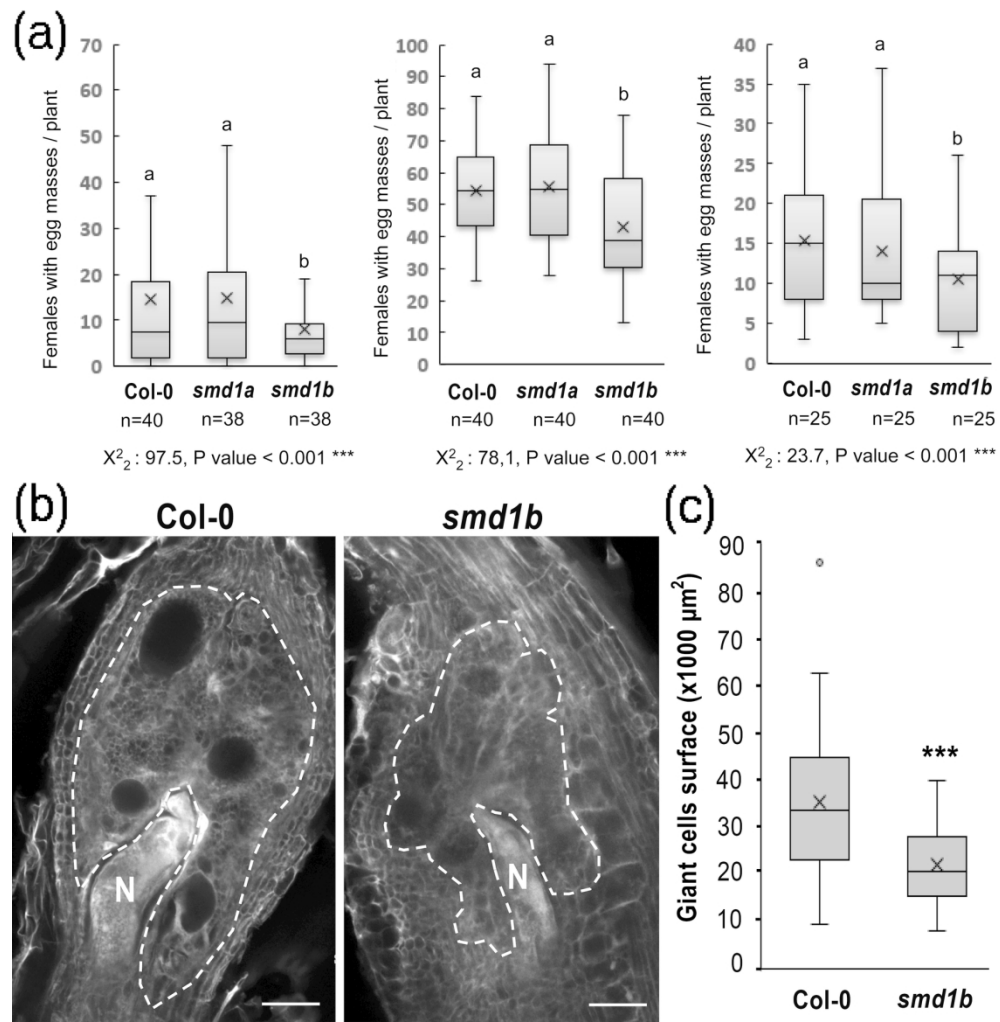


Figure 5

80x81mm (600 x 600 DPI)